Development and validation of a novel technique for murine first-pass radionuclide angiography with a fast multiwire camera and tantalum 178

Jeffrey L. Lacy, PhD, Tamanna Nanavaty, PhD, Dayang Dai, MS, Nisha Nayak, BA, Neal Haynes, BS, and Christopher Martin, AA

Background. **The use of genetically altered mice as a model system to study cardiovascular disease has created a need for accurate and quantitative assessment of murine ventricular function. To address this very challenging problem, we have developed a technique of murine first-pass radionuclide angiography using pinhole imaging and the short-lived isotope tantalum 178 (Ta-178) with a high-speed multiwire proportional camera (MPC).**

Methods and Results. **An MPC was fitted with a pinhole lens of 2-mm-diameter aperture positioned 15 cm from the camera face. The short-lived isotope Ta-178 (half-life 9.3 minutes) was generated from the tungsten 178 (W-178) (half-life 21.7 days)/Ta-178 generator and concentrated on site to an injection volume of 15 to 20 μL. Mice were imaged in the supine position with the chest wall 3 mm from the camera pinhole aperture, and images were acquired at 160 frames per second after a rapid bolus injection of Ta-178. In the absence of a true gold standard, the technology was validated with measurements in control mice and mice with surgically ligated left anterior descending arteries (LADs). In addition, the effects of pharmacologic intervention with verapamil and with dobutamine were observed. Finally, peak aortic velocity measurements obtained with this technology were compared with those obtained with echocardiographic Doppler ultrasonography, the only available quantitative comparator. There was a significant decrease in the mean left ventricular ejection fraction (LVEF) between normal mice (62% ± 4.6% [mean ± SEM], n = 12) and mice with experimentally induced myocardial infarction produced by surgical LAD ligation (22% ± 2.0%, n = 41; $P < .01$). The LVEF decreased from 51% ± 5.8% to 37% ± 3.5% in a group of normal mice receiving verapamil ($P < .05$, n = 8) and increased from 34% ± 2.2% to 43% ± 2.3% in a group of LAD-ligated mice receiving dobutamine ($P < .01$, n = 48). Peak camera sensitivity during first pass was 25,000 cps/mCi injected. Intraobserver and interobserver variability of LVEF was studied, yielding $r = 0.9639$ and 0.9529 and SE of the estimate 2.6% and 3.1%, respectively. Reproducibility in serial studies was excellent ($r = 0.92$, SE of the estimate 5.18).**

Conclusions. **This study demonstrates the development and use of a promising new method that uses the short-lived radioisotope Ta-178 and MPC for noninvasive quantification of murine ventricular function, that produces accurate and highly reproducible results, and that can be applied in multiple serial studies. (J Nucl Cardiol 2001;8:171-81.)**

Key Words: First pass • radionuclide angiography • murine imaging • tantalum 178 • left ventricular ejection fraction

From Proportional Technologies, Inc, Houston, Tex.

The device described here was developed under National Institutes of Health grant R44-HL57086. The work at Baylor College of Medicine was supported by National Institutes of Health grants P01-HL42550 and R37-HL22512 and the DeBakey Heart Center.

Received for publication Feb 23, 2000; final revision accepted Sept 25, 2000.

Reprint requests: Jeffrey L. Lacy, PhD, Proportional Technologies, Inc, 8010 El Rio, Houston, TX 77054; *protecinc@compuserve.com.*

1071-3581/2001/$35.00 + 0 **43/1/112135**

doi:10.1067/mnc.2001.112135

Genetically altered small animals provide a powerful model system for the study of the pathophysiology of cardiac diseases.[1-13] In comparison with destructive ex vivo or in vitro tissue assays, noninvasive imaging can be an extremely useful tool in such studies, facilitating serial assessment in a single animal and thus substantially reducing the cost and time scale of studies. It is not surprising, then, that a considerable amount of effort has gone into developing new techniques for cardiac imaging in small animals.[14-23] Imaging techniques are also being

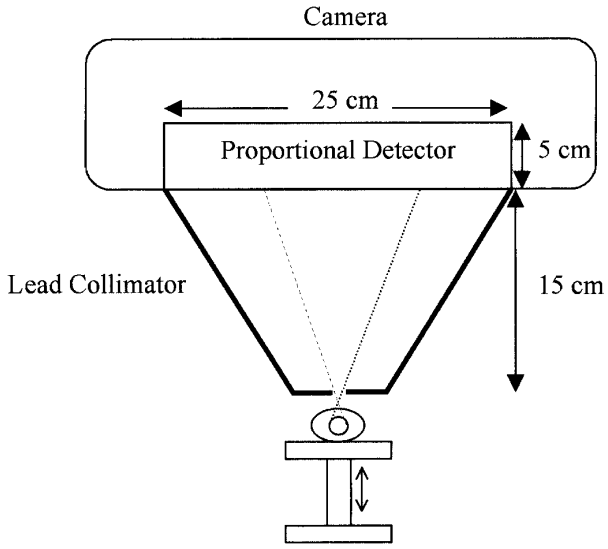

Figure 1. Murine pinhole imaging geometry.

used in the assessment of a wide variety of other organs and diseases.[24-42] Mice prove to be particularly well suited for such work, given our vast knowledge of the mouse genome, the low cost of the operation, and the ability to perform serial studies for relatively short time periods. However, quantification of ventricular function in mice has proved to be exceptionally challenging because of the very small ventricular diameter of 5 mm and the very high heart rate of 600 beats per minute (bpm) in a resting mouse.

We describe the development and validation of a low-cost, compact imaging system that uses the short-lived isotope tantalum 178 (Ta-178) (half-life [$t_{1/2}$] = 9.3 minutes) and a multiwire proportional camera (MPC) equipped with pinhole collimation for assessment of murine ventricular function by first-pass radionuclide angiography (FPRA). The MPC has been extensively used with FPRA in clinical settings and has a number of advantages over conventional gamma cameras, which makes it highly beneficial in the application of murine imaging.[43-52] In particular, it has substantially higher count-rate capability (850,000 cps) and improved intrinsic spatial resolution of 2.5 mm.[43-45] Initial feasibility and validation studies investigating the MPC for this application have been reported previously.[53] Since that study, substantial improvements aimed at enhanced utility and higher reproducibility between studies have been incorporated into the system. A novel automated microscale column concentration procedure that achieves practical concentration of Ta-178 down to a very small volume (much less than the ventricular stroke volume of ~35 μL), which is necessary for first-pass imaging in mice, was developed and is reported here. A pendulum-injector system was developed to enable reproducible and rapid bolus injection. Also unique to this study, interobserver and intraobserver variability was investigated, and left ventricular ejection fraction (LVEF) was compared with Doppler ultrasonographic aortic flow velocity measurements to assess the relative merits and sensitivities of the 2 techniques. Because of the absence of an acceptable gold standard, validation was addressed by assessment of ventricular functional measurements against expected response to surgical and pharmacologic interventions. These data expand on previously reported data.[53]

METHODS

Camera Design and Imaging Characteristics

For murine imaging, the mobile camera, previously used for human FPRA, was reconfigured into a bench-top system fitted with a pinhole collimator of 2-mm-diameter aperture positioned 15 cm from the image plane. In this manner an enlarged image of the mouse heart was projected on the 25-cm-diameter field of view of the MPC. A cross-sectional schema of the system is shown in Figure 1. The mice were anesthetized and placed in the supine position under the pinhole aperture. The distance between the face of the pinhole and the ventricular centroid was adjusted to approximately 1 cm, providing 15-fold magnification. We accomplished this in practice with reasonable reproducibility by placing the surface of the pinhole aperture 3 mm from the surface of the mouse chest wall, using a 3-mm spacer for verification. A frame rate of 160 frames per second was used (compared with 40 frames per second used for human imaging) to obtain, on average, 16 frames per cardiac cycle, given a heart rate of 600 bpm (10 beats per second).

Spatial Resolution and Scatter

In the murine FPRA studies, the vast majority of the actual injected dose was in the heart chambers during the relevant imaging period. An average of 0.7 cm of tissue was traversed between the heart and the pinhole. Only 13% of the 60-keV Ta-178 x-rays interacted in this thin tissue layer, and because most of the resulting radiation was scattered out of the acceptance aperture of the collimator, it interfered very little with the image. In the backward direction, 2 to 3 cm of tissue was traversed, producing a 33% to 45% interaction probability. However, most of this low-level scatter was produced at significantly deeper levels (further from the pinhole) and therefore was imaged with much lower sensitivity. Thus the contribution of scatter in the images was low and varied over the image by a very small percentage, allowing effective removal by background subtraction.

Ta-178 Generator/Concentrator

The development of an automated, portable tungsten 178 (W-178)/Ta-178 generator system for clinical use has been described in detail elsewhere.[52,54-56] With this generator, 1.5 mL of dilute hydrogen chloride (0.03 mol/L) eluant was passed

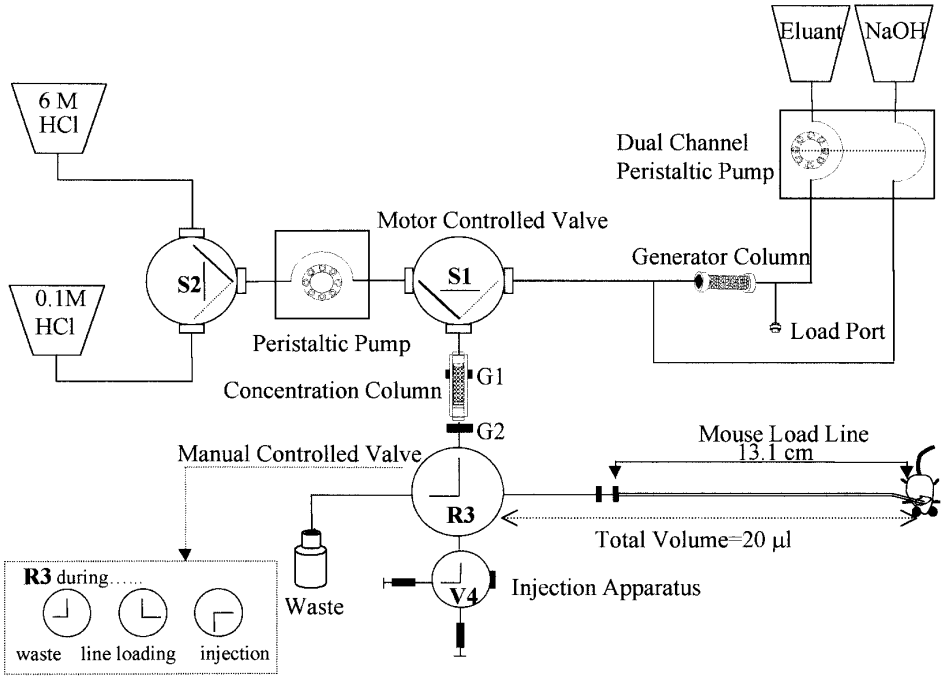

Figure 2. Schema of the murine imaging system, composed of the generator module, the concentration module, and the injection apparatus. Ta-178 is eluted from the generator column by activation of the peristaltic pump as shown above. The generator output is directed to the concentration module at one input to the solenoid valve *(S1)*. This valve directs flow through the 5-µL microcolumn *(Concentration Column)* to a motor-controlled valve *(R3)*, which in turn directs flow from the column either to the waste reservoir or to the mouse load line during elution of the column. Two miniature Geiger probes (*G1* and *G2*) monitor activity trapped on the concentration column and the wash-off profile, respectively. The activity profiles of the Geiger probes are followed on a computer monitor in real time. During column elution, valve R3 is programmed to turn and connect the column to the load line at a calculated count threshold, as set in the software, directing most of the peak concentrated activity to the load line. The generator elution, Ta-178 concentration, valve operation, and monitoring of the Geiger probes are fully automatic and controlled by an online computer.

over an anion-exchange column that was loaded with the parent isotope, W-178 ($t_{1/2}$ = 21.7 days), to extract the daughter isotope, Ta-178 ($t_{1/2}$ = 9.3 minutes). Subsequent in-line addition of 0.15 mol/L NaOH facilitated efficient trapping of the Ta-178 onto a specially designed microscale anion-exchange column with a bed volume of 5 µL (Figure 2). The microscale column was eluted with 0.1 mol/L HCl to obtain a concentrated Ta-178 bolus. Elution proceeded until a 20-µL volume of Ta-178 solution (~20 mCi) was delivered to the load line, sized to hold that exact volume. This entire procedure was controlled by customized Windows-based software. A schema of the overall system configuration is shown in Figure 2.

Injection System Configuration

During the feasibility studies, injections were performed manually.[53] For a more repeatable rapid injection with a consistent bolus time profile, activation of the syringe plunger at a fixed, reproducible velocity was required. Therefore a microinjection apparatus and technique were developed with a weighted pendulum that was released from a fixed distance, activating the Hamilton syringe plunger, as shown in Figure 3. A pendulum's velocity at the bottom of its travel is independent of its weight and depends only on its length, allowing independent adjustment of injection velocity and force. The horizontal velocity *(V)* of the pendulum striking the plunger is given by $V \cong (g/L)^{1/2} * (X)$, where g is the gravitational constant, L is the pendulum length, and X is the initial horizontal displacement. The required 20-µL injection volume corresponded to a 2.5-cm plunger displacement. Thus the delivery of this volume in 0.1 second required a velocity of 25 cm/s. A pendulum length of 30 cm was used, so solving for X, the horizontal displacement needed to achieve this velocity was 4.5 cm (Figure 3). Simple adjustment of the initial pendulum displacement easily enabled modifications around this delivery speed.

Injection Procedure

The reproducibility of injections with the pendulum system was compared with that of manual injections. Manual injections were performed by a separate observer 8 months before the development of the pendulum injector. Ten studies having good technical quality were selected at random. From each data set, a plot of total image counts collected by the MPC versus raw frame number (6.25 ms/frame) was created for each study. Each curve was then smoothed with a finite impulse response (FIR) low-pass filter with a cutoff of 0.2π Hz to remove high-frequency fluctuations. The rise time was calcu-

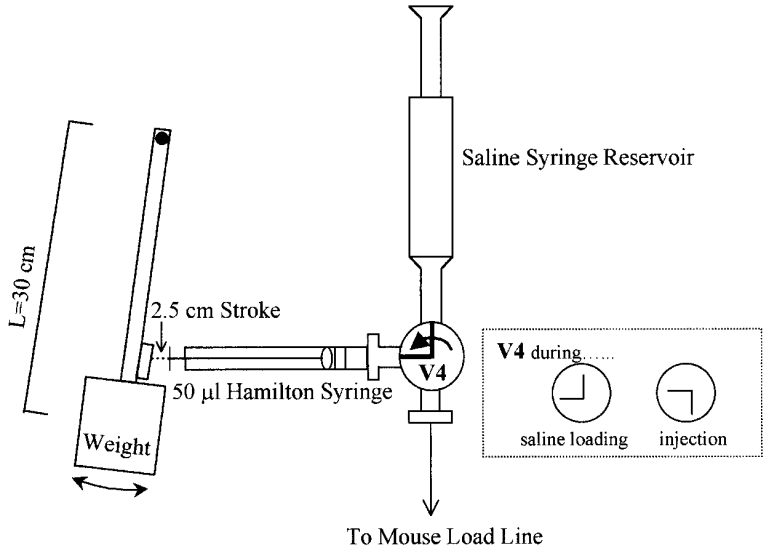

Figure 3. The injection apparatus is a 4-component system containing a 50-µL Hamilton syringe, a saline solution reservoir, a pendulum, and an injector line connecting to the mouse jugular line. After elution of concentrated Ta-178, the manually controlled valve *(V4)* is repositioned by the operator. This valve connects the injector to the mouse load line, and injection and image acquisition are performed. *L,* Pendulum length.

lated as the time taken for counts to increase from 10% of maximum to 90% of maximum.

Imaging Protocol

All animal protocols were approved by the Institutional Animal Care and Use Committees of the American Association for Accreditation of Laboratory Animal Care (accredited institution Baylor College of Medicine), in accordance with the National Institutes of Health *Guide for the Care and Use of Laboratory Animals.*[57] Mice were anesthetized with 0.2 to 0.4 mL of pentobarbital sodium solution (4 mg/mL) given intraperitoneally. Additional anesthetic in 0.05-mL increments was administered during image acquisition if needed (as judged by tail reflex). After cannulation of the right jugular vein with a fine-gauge catheter (PE10), the mouse was placed in the supine position on a specially designed board to provide immobilization, to monitor electrocardiographic (ECG) signals, and to regulate body temperature as shown in Figure 4. The board was constructed with dual connections to a temperature monitor and an ECG amplifier. Body temperature was monitored with a rectal probe. The head was constrained with sutures around the canine teeth to maintain proper body alignment. The ECG signals were obtained from the left and right front feet, with the rear feet providing a common ground. The electrocardiogram was monitored on an oscilloscope to allow continuous observation of the mouse's physiologic status. For injection and study acquisition, the mouse was positioned on a support jack, providing fine vertical adjustment, below the pinhole lens of the MPC lead collimator. A cross was drawn on the mouse's chest approximating the position of the centroid of the heart, and the center of the cross was aligned with the center of the pinhole. Spacing of 3 mm from the pinhole to the chest surface was set as previously described to provide 15-fold magnification of the heart.[53] The Ta-178 injection levels ranged from 10 to 20 mCi. When obtaining multiple images in the same mouse, we allowed an interval of 30 to 45 minutes between studies to permit substantial decay of Ta-178 from the previous injection and to allow optimal buildup of the W-178/Ta-178 generator.

Study Population

All imaging was performed on C57-strain mice ranging from 15 to 40 g in weight and from 3 to 12 months in age. In the drug intervention studies, a total of 45 mice were imaged, including 23 mice with experimentally induced myocardial infarction produced by surgical left anterior descending artery (LAD) ligation (LAD-ligated mice),[58] 10 mice with related surgical trauma but no coronary ligation (sham-operated mice), and 12 normal mice. A total of 15 LAD-ligated mice and 6 sham-operated mice were studied at baseline and with dobutamine infusion. A group of 6 normal mice was studied at baseline and with verapamil infusion. Interobserver and intraobserver variability comparisons were performed in a second group of mice. A total of 34 mice were imaged in this second group, including 24 LAD-ligated mice, 7 sham-operated mice, and 3 normal mice. Reproducibility studies were performed in mice from both groups, including a total of 5 normal mice, 15 LAD-ligated mice, and 3 sham-operated mice. Doppler ultrasonographic measurements were performed in mice from both groups; a total of 12 normal mice, 14 sham-operated mice, and 41 LAD-ligated mice were used.

Image Processing and Analysis

Image processing of the MPC/Ta-178 first-pass studies with specially designed software has been previously described.[50] Processing with this software was performed in 3 to 5 minutes

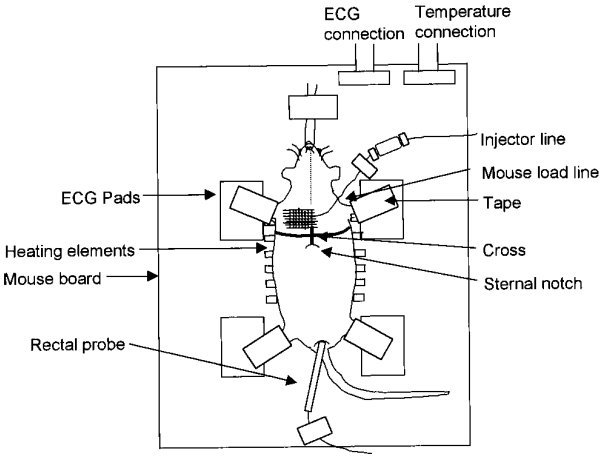

Figure 4. Illustration of an anesthetized mouse oriented in the supine position and taped to a specially designed mouse board with dual connections to the ECG amplifier and temperature controller. All 4 feet are securely taped to ECG electrode pads with conductive gel, providing secure electrical contact.

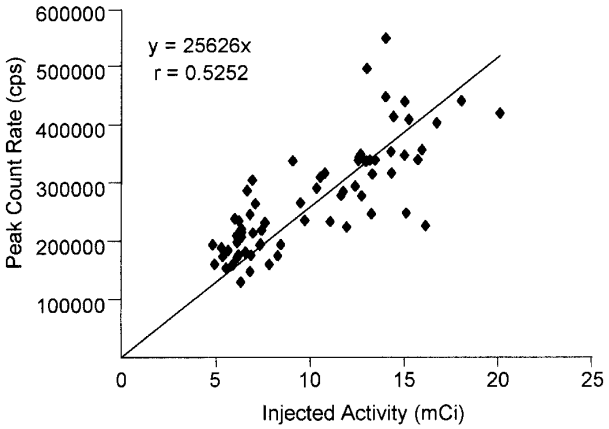

Figure 5. Relation between peak count rate from the MPC and the injected Ta-178 activity. A linear regression yields a slope of 25,626 cps/mCi. No sign of saturation up to 20 mCi is seen.

to obtain left ventricular (LV) representative cardiac cycle images, time-activity curves, and LVEF. In addition to quantitative information, LV cinematic images were displayed side by side on a high-resolution color display to allow visual analysis of ventricular wall motion. An experienced observer reprocessed 34 first-pass studies 1 month after the original processing so that intraobserver reproducibility of LVEF could be evaluated. The interobserver reproducibility was assessed by having a second experienced blinded observer reprocess these studies independently of the first observer.

Doppler Procedure

Doppler ultrasonography was performed either 24 hours or 1 to 2 hours before the FPRA study.[59,60] Mice were anesthetized by an intraperitoneal injection of a mixture of 1.4 mg/mL acepromazine, 8.6 mg/mL xylazine, and 42.6 mg/mL ketamine at a dose of 0.5 µL/g body weight. They were taped to a temperature-controlled laminated plastic board, with copper electrodes placed such that the 3 bipolar limb leads allowed ECG monitoring. Body fur at the left lower sternal border was clipped lightly, and the skin in that area was wetted with warm water to improve sound transmission. A 10-MHz pulsed Doppler probe was positioned just below the xiphoid, with the gate depth set at 7 mm to obtain aortic outflow signal. The Doppler module generated a pulse-repetition frequency of 62.5 kHz, allowing Doppler shifts of up to 31.25 kHz to be resolved without aliasing. The Doppler shifts were measured in frequency (kilohertz) and were converted into velocity (centimeters per second) by multiplication of the frequency in kHz by 7.7 cm/s/kHz for 10-MHz Doppler. The speed of sound in soft tissue was taken as 1540 m/s, and the incident angle of the Doppler signal was assumed to be close to zero. The quadrature Doppler audio signals were entered into a real-time fast Fourier transform spectrum analyzer. The spectrum analyzer converted the signals into a frequency spectrogram, which is the representation of the time-based velocity signal of aortic blood flow. An average peak velocity from 10 to 15 beats from the spectrogram of each mouse was calculated in centimeters per second.

RESULTS

Image Quality

A graph of the peak count rate obtained from each study in the first population of mice versus the decay-corrected injected activity is shown in Figure 5. The slope of the correlation line gives an overall sensitivity of the pinhole collimator of 25,626 cps/mCi. It is notable that this measured sensitivity is only marginally lower than the 33,000 cps/mCi obtained with the same detector and the parallel-hole collimator used for human imaging. The maximum injected activity of 20 mCi provided a peak count rate of 500,000 cps, which is well below the saturation count rate of the MPC of 850,000 cps, introducing acceptable dead-time losses of less than 30%.[46] The camera peak count rate is inversely proportional to the square of the distance from the mouse heart to the face of the pinhole, which was manually adjusted during experiments, explaining the deviation of data points from the regression line in this plot.

Mouse Physiology and Modification of First-Pass Processing

Figure 6 shows the first cardiopulmonary transit of activity in a typical first-pass study performed in a normal 24-g mouse with a heart rate of 533 bpm. The sequential images from left to right and from top to bottom are frames averaged at end diastole of successive heartbeats. The first 6 frames show the bolus entry and transit of the radioisotope through the right side of

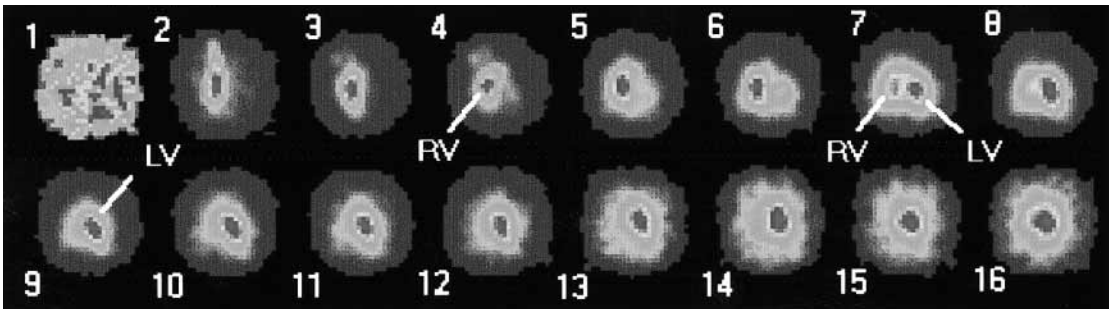

Figure 6. Sequential images corresponding to frames averaged at end diastole of successive heartbeats are shown for a normal 25-g mouse (heart rate 600 bpm) injected with 15 mCi of Ta-178. Bolus entry *(frame 1)* and transit of the radioisotope through the right side of the heart occur in 6 heartbeats. The activity quickly appears in the left ventricle *(LV) (frame 7).* A clear separation of both ventricles is also seen in this frame. *RV*, Right ventricle.

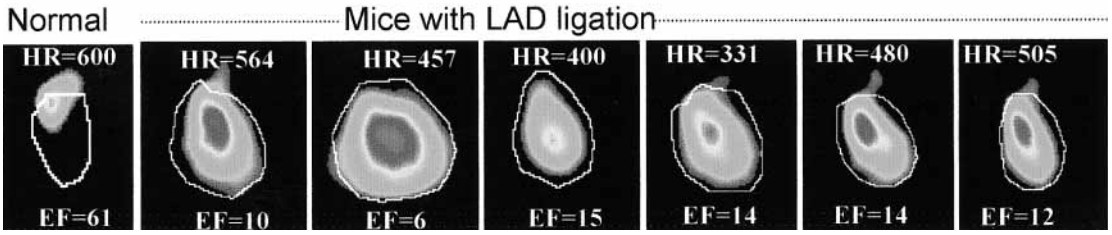

Figure 7. End-diastolic perimeter *(white border)* superimposed on end-systolic ventricular images of a normal mouse *(far left)* and 6 representative LAD-ligated mice is shown. Heart rate *(HR)* is given at the *top,* and LVEF measurements are given at the *bottom.*

Table 1. Mean LVEF and mean peak aortic velocity values of normal, sham-operated, and LAD-ligated mice

Group	Mean LVEF (%)	Mean peak aortic velocity (cm/s)
Normal (n = 12)	62 ± 4.6	104.3 ± 2.8
Sham-operated (n = 14)	43 ± 3.2 ($P < .01$ vs normal)	89 ± 4.1 ($P < .01$ vs normal)
LAD-ligated (n = 41)	22 ± 2.0 ($P < .01$ vs normal) ($P < .01$ vs sham-operated)	94 ± 2.9 ($P < .05$ vs normal) (P = NS vs sham-operated)

NS, Not significant.

the heart; the activity then appears in the left ventricle (frame 7). Because of the posterior position of the lungs in the mouse, the pulmonary background is largely absent. A clear separation of the 2 ventricles can also be observed in this frame. The clear definition of ventricles separated only by the thin septum is a notable demonstration of the superior spatial resolution of the technique.

Functional Effect of Surgical Interventions and Comparison With Peak Aortic Flow Velocity Measurements

Figure 7 shows the end-diastolic perimeter superimposed on the end-systolic image for a normal mouse and several LAD-ligated mice. A considerable increase in the relative LV volume and a marked decrease in LVEF are apparent in LAD-ligated versus normal mice. A scatter plot of peak aortic velocity versus LVEF obtained from the same groups of mice used to study the functional effects of surgical intervention is shown in Figure 8. Measurements of normal, sham-operated, and LAD-ligated mice from both groups (the first group used in part for drug intervention studies and the second group used to assess interobserver and intraobserver variability) are compared. Mean peak aortic velocity and mean LVEF of normal, sham-operated, and LAD-ligated mice are shown in Table 1. A significant 65% decrease in mean LVEF of the normal mice (n = 12) versus the LAD-ligated mice (n = 41) was seen (from 62% ± 4.6% [mean ± SEM] to 22% ± 2.0%, $P < .01$). The

peak aortic velocity decreased by only 10% (from 104.3 ± 2.8 to 94 ± 2.9 cm/s, $P < .05$). In contrast, LVEF measurements decreased by 30% in sham-operated mice (n = 14) compared with those in normal mice (n = 12) (from 62% ± 4.6% to 43% ± 3.2%, $P < .01$), and peak aortic velocity decreased by 14% in these mice (from 104.3 ± 2.8 to 89 ± 4.1 cm/s, $P < .01$). This drop is believed to be a result of myocardial adhesions produced by surgical trauma, which were also observed in some animals in the FPRA study as clearly evident regional ventricular abnormalities. A significant drop in LVEF was seen between sham-operated and LAD-ligated groups of mice (from 43% ± 3.2% to 22% ± 2.0%, $P < .01$). However, there was no distinguishable difference in aortic velocity between sham-operated and LAD-ligated mice (89 ± 4.1 and 94 ± 2.9 cm/s, not significant).

Functional Effect of Pharmacologic Interventions

Individual paired LVEF values of LAD-ligated and normal mice at baseline and after intervention are shown in Figure 9*A* and *B*. With dobutamine, the LVEF increased in the LAD-ligated group from 34% ± 2.2% to 43% ± 2.3% ($P < .01$, n = 48). With verapamil, the LVEF decreased in the normal group from a baseline value of 51% ± 5.8% to 37% ± 3.5% ($P < .05$, n = 8). Wall motion abnormalities seen in mice with evidence of aneurysm were often enhanced with dobutamine. Dobutamine infusion had similar effects on the ventricular function of sham-operated and LAD-ligated mice. Verapamil infusion caused a decrease in LVEF and LV peak ejection rate and an increase in LV end-systolic volume in sham-operated mice. The LV time-activity curves of a sham-operated mouse at baseline and with dobutamine intervention and a sham-operated mouse at baseline and with verapamil intervention are shown in Figure 10*A* and *B*, respectively. An increase in LVEF with dobutamine compared with baseline is seen, with an accompanying increase in the LV peak ejection rate. An increase in myocardial contractility and a substantial decrease in LV volume at end systole with dobutamine are also visible.

Reproducibility of Serial LVEF Measurements

The first and second LVEF measurements of normal, sham-operated, and LAD-ligated mice are compared in Figure 11. Good agreement between the successive LVEF measurements is seen (n = 23, $r = 0.86$, SE of the estimate [SEE] = 5.18).

Intraobserver and Interobserver Variability of LVEF

In Figure 12*A*, interobserver variability statistical analysis of LVEF yielded $r = 0.9529$ and SEE = 3.05. In Figure 12*B*, intraobserver variability analysis of LVEF yielded $r = 0.9639$ and SEE = 2.65.

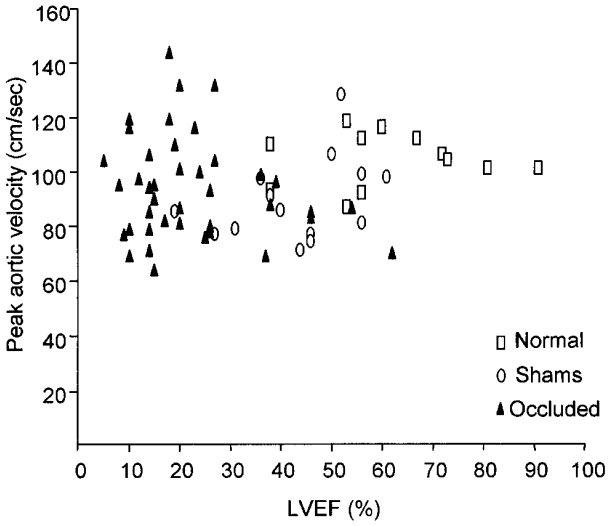

Figure 8. Relation between LVEF and peak aortic velocity obtained by Doppler ultrasonography from normal mice, sham-operated mice, and LAD-ligated mice.

Evaluation of Pendulum Injector

Bolus time profiles of the pendulum injection method are compared with those of the manual injection method in Figure 13*A* and *B*. The 10% to 90% bolus entry time calculated for the 10 manual injection studies was 164 ± 64 ms (mean ± SD) (range 38-256 ms), and that for 10 pendulum injections was 134 ± 29 ms (range 81-169 ms). Although the decrease in rise time was not found to be statistically significant, injection times were far more consistent with use of the automated system, as demonstrated by the greatly reduced variance ($F = 4.87$, $P < .05$).

DISCUSSION

The development and use of a novel noninvasive murine cardiovascular imaging system that provides rapid and reproducible evaluation of murine ventricular function have been demonstrated in this report.[53] High-quality images were obtained in first-pass studies, providing assessment of wall motion, global and regional LVEF measurements, and qualitative estimation of ventricular volume. Validation of the system was performed with 3 kinds of interventions: surgically induced myocardial infarction, a positive inotropic agent, and a negative inotropic agent.[53] A substantial decrease in LVEF and severe wall motion abnormalities were consistently observed in LAD-ligated mice compared with normal mice. Dobutamine in these mice produced an increase in

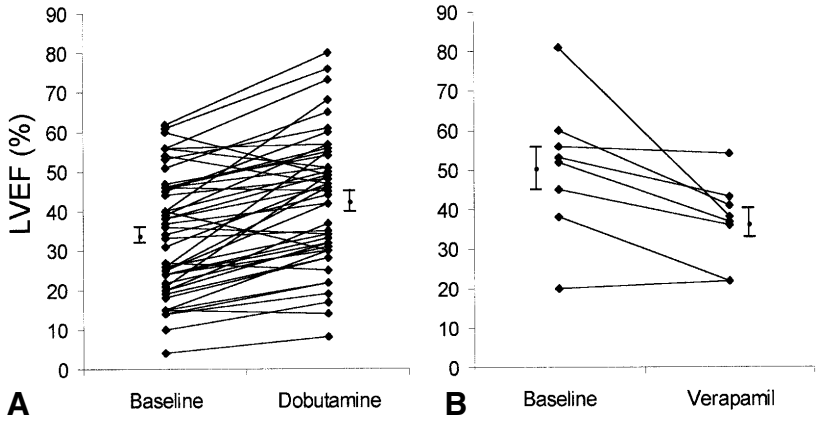

Figure 9. A, Individual paired LVEF values of LAD-ligated mice at baseline and after dobutamine intervention. **B,** Individual paired LVEF values of normal mice at baseline and after verapamil intervention.

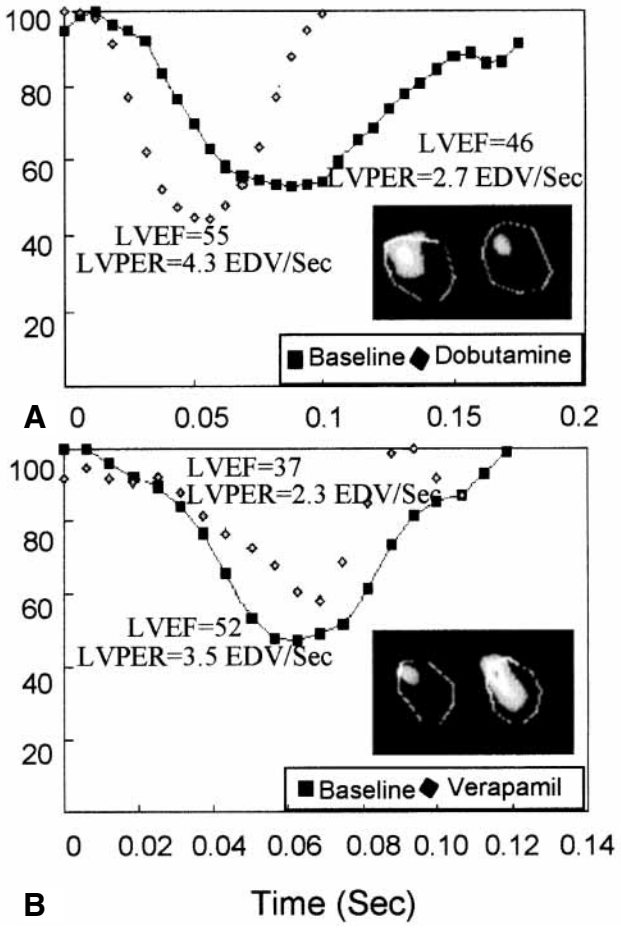

Figure 10. Examples of the effect of pharmacologic interventions on ventricular function of mice. Time-activity curves of a sham-operated mouse at baseline and with dobutamine intervention **(A)** and a sham-operated mouse at baseline and with verapamil intervention **(B).** *Insets,* Corresponding ventricular images at baseline and with intervention. Images display end-diastolic perimeter superimposed on end-systolic ventricular image. *LVPER,* LV peak ejection rate; *EDV/Sec,* end-diastolic volume per second.

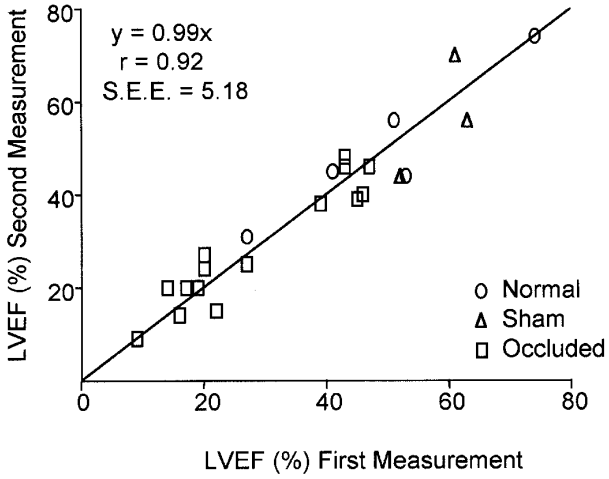

Figure 11. Plot of successive serially measured LVEF demonstrating the reproducibility of the method.

LVEF and regional myocardial contractility, often accentuating wall motion abnormalities in cases in which there was evidence of aneurysm. Verapamil produced a substantial decrease in LVEF compared with baseline in both normal and sham-operated mice. These results are consistent with the well-documented response to these interventions in large animals and human beings.[53] The drop in peak aortic flow velocity of LAD-ligated mice compared with that of normal mice was much less than the reduction in LVEF of the same groups, suggesting that the Doppler ultrasound method is relatively insensitive compared with LVEF measurements in such a population. Stroke volume and cardiac output remain nearly normal despite the lowered LVEF because of the compensatory effects, which keep aortic output velocity relatively unchanged. This demonstrates that FPRA provides a substantially more complete characterization of the

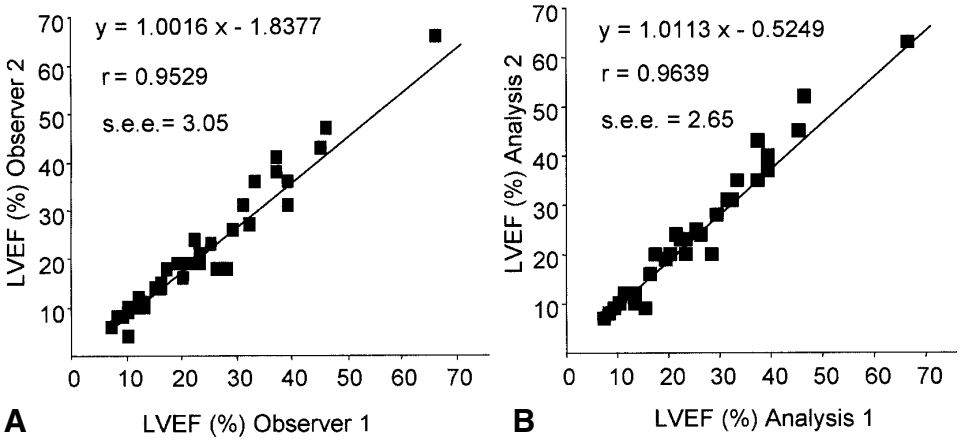

Figure 12. Interobserver **(A)** and intraobserver **(B)** variability of LVEF is shown, as obtained by reprocessing a range of first-pass studies.

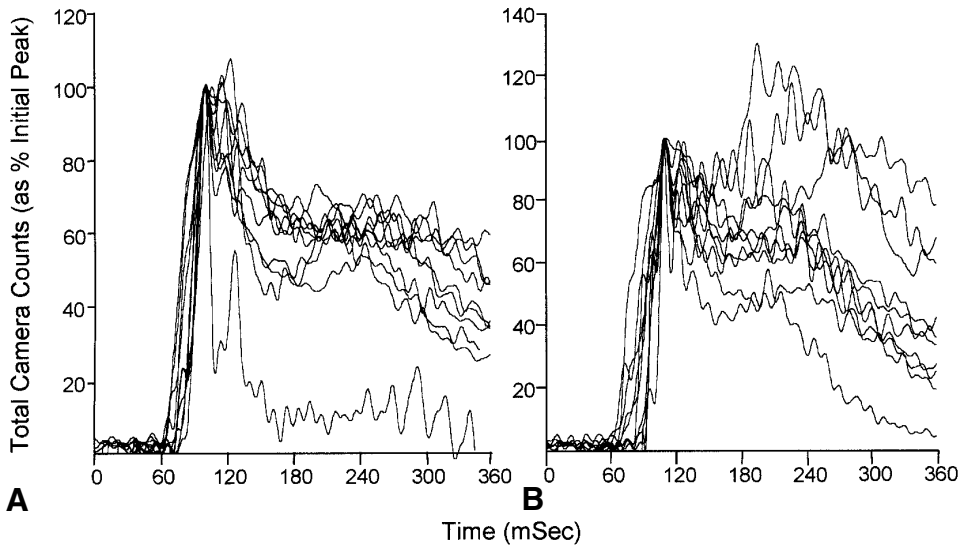

Figure 13. Examples of bolus time profiles with the pendulum injector **(A)** and manual injections **(B)** are shown.

coronary occlusion model in mice. In addition, a statistically significant difference was observed in LVEF of sham-operated and LAD-ligated mice, but there was no statistically significant difference between peak aortic flow velocities in these groups. This implies that peak aortic flow velocity may be more influenced by surgical trauma. The reproducibility of successive LVEF measurements as well as interobserver and intraobserver processing variability was excellent. Results from the evaluation of the pendulum injection method demonstrated considerably improved bolus speed and reproducibility compared with manual method.

Modern techniques for studying cardiovascular function, such as magnetic resonance imaging (MRI),[17-19] echocardiography,[20-22] and x-ray contrast angiography,[23] are well developed in large animals, but in the mouse, these techniques are pushed to the limits of spatial and temporal resolution.[53] When 2-dimensional echocardiography is adapted for a mouse model, the rapid heart rate of the animal typically exceeds the resolution capability of a standard 7-MHz transducer.[1] With the frame rate of 30 frames per second and an average mouse heart rate of 600 bpm, each frame represents one third of a heartbeat, providing clearly inadequate temporal resolution.[1] Advances in echocardiography equipment, such as high-frequency (9 to 11 MHz) transducers, provide improved spatial resolution and frame rate in mice, but drawbacks include considerable interobserver error and limited accuracy in volume measurements due to ventricular geometry assumptions.[1,20] Recently, myocardial contrast echocardiography

has been successfully used in mice. However, drawbacks include lack of reliability of the algorithm in following the rapid mouse heart rate, tedious manual tracing of the endocardial boundary in image analysis, and limited frame rate.[20,61] X-ray contrast microangiography has also been adapted in mice, but it is invasive and also severely limited in temporal resolution.[23] Only recently, a high-field strength cine MRI system (7.05 T) with high spatial and temporal resolution for quantification of murine cardiac mass and function has been reported.[1,62] Excellent cine images and measurements of ventricular volume, ejection fraction, and ventricular mass were obtained with this system. However, a cine frame rate of only 12 frames per heartbeat was achieved at a lowered mouse heart rate of 370 bpm produced by anesthetic effects.[61] For mice with a normal heart rate of 600 bpm as studied here, this temporal resolution is thoroughly inadequate, providing only 7 frames per heartbeat. The MPC system, on the other hand, provides 16 frames per heartbeat, and there is no intrinsic barrier to even higher frame rates with this technique. Finally, the cost of the ultra-high-field strength MRI systems (half a million dollars) is on the order of 10 times that of the MPC, and because there is not a base of clinical systems, they suffer from lack of widespread availability.

A potentially serious drawback of the FPRA technique in murine imaging—inadequate bolus delivery—has been resolved by the development of an automated concentrator and a pendulum-injector system, which provide highly reproducible studies. For the first time, this technology has demonstrated the capability of providing excellent ventricular function measurements in mice at physiologic heart rate with desired spatial and temporal resolution. The MPC is also inexpensive, allowing widespread application of the powerful cardiovascular models afforded by genetically altered mice.

We thank Jennifer Pocius for performing animal surgery and Anil Reddy, PhD, for technical assistance and echocardiographic Doppler measurements, and we would like to convey special thanks to Lloyd Michael, PhD, Craig Hartley, PhD, and Mark Entman, MD, PhD, for their invaluable support and advice in development and validation of the technique. All are from the Department of Medicine, Section of Cardiovascular Sciences, Baylor College of Medicine, Houston, Tex.

References

1. James JF, Hewett TE, Robbins J. Cardiac physiology in transgenic mice. Circ Res 1998;82:407-15.
2. Kadambi VJ, Kranias EG. Genetically engineered mice: model systems for left ventricular failure. J Card Fail 1998;4:349-61.
3. Izumo S, Shioi T. Cardiac transgenic and gene-targeted mice as models of cardiac hypertrophy and failure: a problem of (new) riches. J Card Fail 1998;4:263-70.
4. Arbeit JM, Hirose R. Murine mentors: transgenic and knockout models of surgical disease. Ann Surg 1999;229:21-40.
5. Carmeliet P, Moons L, Collen D. Mouse models of angiogenesis, arterial stenosis, atherosclerosis and hemostasis. Cardiovasc Res 1998; 39:8-33.
6. Lee MA, Bohm M, Bader M, Ganten U, Ganten D. Physiological characterization of the hypertensive transgenic rat TGR(mREN2)27. Am J Physiol 1996;270:E919-29.
7. Paigen B, Plump AS, Rubin EM. The mouse as a model for human cardiovascular disease and hyperlipidemia 1994;5:258-64.
8. French BA. Gene transfer and cardiovascular disorders. Herz 1993;18: 222-9.
9. Murakami K, Fukamizu A. Transgenic and knockout models in renin-angiotensin system. Immunopharmacology 1999;44:1-7.
10. Verdouw PD, van den Doel MA, de Zeeuw S, Duncker DJ. Animal models in the study of myocardial ischaemia and ischaemic syndromes. Cardiovasc Res 1998;39:121-35.
11. Drago JPA, Accili D, Eisner GM, Felder RA. Transgenic mice to study the role of dopamine receptor in cardiovascular function. Clin Exp Hypertens 1997;19:15-25.
12. Young SG. Using genetically modified mice to study apolipoprotein B. J Atheroscler Thromb 1996;3:62-74.
13. Penninger LP, Aitken K, Sole M, Mak T. The role of transgenic knockout models in defining the pathogenesis of viral heart disease. Eur Heart J 1995;16:25-7.
14. Waldenstrom A, Langstrom B. Assessment of cardiac metabolic disorders with positron emission tomography. Curr Opin Cardiol 1991;6: 965-71.
15. Garlick PB, Marsden PK, Cave AC, Parkes HG, Slates R, Shao Y. PET and NMR dual acquisition (PANDA): application to isolated, perfused rat hearts. NMR Biomed 1997;10:138-42.
16. Shimada K, Yoshida K, Tadokoro H, Kitsukawa S, Takami A, Susuki K. High-resolution cardiac PET in rabbits: imaging and quantitation of myocardial blood flow. J Nucl Med 1998;39:2022-7.
17. Yoshida S, Dodd SJ, del Nido PJ, Williams DS, Ho C. Cardiac function of transplanted rat hearts using a working heart model assessed by magnetic resonance imaging. J Heart Lung Transplant 1999;18:1054-64.
18. Franco F, Dubois SK, Peshock RM, Shohet RV. Magnetic resonance imaging accurately estimates LV mass in transgenic mouse model of cardiac hypertrophy. Am J Physiol 1998;274:H679-83.
19. Franco F, Thomas GD, Giroir B, Bryant D, Bullock MC, Chwialkowski MC, et al. Magnetic resonance imaging and invasive evaluation of development of heart failure in transgenic mice with myocardial expression of tumor necrosis factor-alpha. Circulation 1999;99:448-54.
20. Mor-Avi V, Korcarz C, Fentzke RC, Lin H, Leiden JM, Lang RM. Quantitative evaluation of left ventricular function in a transgenic mouse model of dilated cardiomyopathy with 2-dimensional contrast echocardiography. J Am Soc Echocardiogr 1999;12:209-14.
21. Williams RV, Lorenz JN, Witt SA, Hellard DT, Khoury PR, Kimball TR. End-systolic stress-velocity and pressure dimension relationships by transthoracic echocardiography. Am J Physiol 1998;274:H1828-35.
22. Manning WJ, Wei JY, Katz SE, Douglas PS, Gwathmey JK. Echocardiographically detected myocardial infarction in the mouse. Lab Anim Sci 1993;43:583-5.
23. Rockman HA, Ono S, Ross RS, Jones LR, Karimi M, Bhargava V, et al. Molecular and physiological alterations in murine ventricular dysfunction. Proc Natl Acad Sci U S A 1994;91:2694-8.
24. Rivers BJ. Diagnostic imaging strategies in small animal nephrology. Vet Clin North Am Small Anim Pract 1996;26:1505-17.
25. Hume SP, Jones T. Positron emission tomography (PET) methodology for small animals and its application in radiopharmaceutical preclinical investigation. Nucl Med Biol 1998;25:729-32.
26. Weber DA, Ivanovic M. Ultra-high-resolution imaging of small ani-

mals: implications for preclinical and research studies. J Nucl Cardiol 1999;6:332-44.
27. Daniel GB, Mitchell SK, Mawby D, Sackman JE, Schmidt D. Renal nuclear medicine: a review. Vet Radiol Ultrasound 1999;40:572-87.
28. Shevelev IA, Tsicalov EN, Gorbach AM, Budko KP, Sharaev GA. Thermoimaging of the brain. J Neurosci Methods 1993;46:49-57.
29. Wolf GL. Technical improvements in the staging of cancer: the role of imaging and contrast agents. Artif Cells Blood Substit Immobil Biotechnol 1994;22:285-94.
30. Bischof DA, Delaloye B. Tumor imaging with monoclonal antibodies. Semin Nucl Med 1995;25:144-64.
31. Chatziioannou AF, Cherry SR, Shao Y, Silverman R, Meadors K, Farquhar TH. Performance evaluation of microPET: a high-resolution lutetium, oxyorthosilicate PET scanner for animal imaging. J Nucl Med 1999;40:1164-75.
32. Jeavons AP, Chandler RA, Dettmar CAR. A 3D HIDAC-PET camera with sub-millimeter resolution for imaging small animals. IEEE Trans Nucl Sci 1999;46:468-73.
33. Moor JV, Waller ML, Zhao S, Dodd NJF, Acton PD, Jeavons AP, et al. Feasibility of imaging photodynamics injury to tumors by high-resolution positron emission tomography. Eur J Nucl Med 1998;25: 1248-54.
34. MacLaren DC, Gambhir SS, Satyamurthy N, Barrio JR, Sharfstein S, Toyokuni T, et al. Repetitive, non-invasive imaging of the dopamine D2 receptor as a reporter gene in living animals. Gene Ther 1999; 6:785-91.
35. Moo AH, Cherry SR, Pollack DB, Hovada DA, Phelps ME. Application of positron emission tomography to determine cerebral glucose utilization in conscious infant monkeys. J Neurosci Methods 1999;88:123-33.
36. Gambhir SS, Barrio JR, Phelps ME, Iyer M, Namavari M, Satyamurthy N, et al. Imaging adenoviral-directed gene expression in living animals with positron emission tomography. Proc Natl Acad Sci U S A 1999;96:2333-8.
37. Cutler PD, Cherry SR, Hoffman EJ, Digby WM, Phelps ME. Design features and performance of a PET system for animal research. J Nucl Med 1992;33:595-604.
38. Cherry SR, Shao Y, Siegel S. Optical fiber readout of scintillator arrays using a multi-channel PMT: a high resolution PET detector for animal imaging. IEEE Trans Nucl Sci 1996;43:1932-7.
39. Cherry SR, Chatziioannou A, Shao Y, Silverman RW, Meadors K, Phelps M. Brain imaging in small animals using MicroPET. In: Carson R, Daube-Witherspoon M, Herscovitch P, editors. Quantitative functional brain imaging with positron emission tomography. San Diego (CA): Academic Press; 1998. p. 3-9.
40. Qi J, Leahy R, Cherry S, Chatziioannou A, Farquhar T. High-resolution 3D Bayesian image reconstruction using the microPET small-animal scanner. Phys Med Biol 1998;43:1001-13.
41. Carrig CB. Diagnostic imaging of osteoarthritis. Vet Clin North Am Small Anim Pract 1997;27:777-814.
42. Li KC. MR angiography of abdominal ischemia. Semin Ultrasound CT MR 1996;17:352-9.
43. LeBlanc AD, Lacy JL, Johnson PC, Poliner LR, Jhingran SG. Tantalum-178 count-rate limitations of Anger and multicrystal cameras. Radiology 1983;146:242-3.
44. Lacy JL, Verani MS, Ball ME, Boyce TM, Gibson RW, Roberts R. First-pass radionuclide angiography using a multiwire gamma camera and tantalum-178. J Nucl Med 1988;29:293-301.
45. Lacy JL, LeBlanc AD, Babich JW, Bungo MW, Laston LA, Lewis RM, et al. A gamma camera for medical applications, using a multiwire proportional counter. J Nucl Med 1984;256:1003-12.
46. Adams R, Lacy JL, Ball ME, Martin LJ. The count rate performance of a multiwire gamma camera measured by a decaying source method with 9.3-minute tantalum-178. J Nucl Med 1990;31:1723-6.
47. Ott RJ. Wire chambers revisited. Eur J Nucl Med 1993;20:348-58.
48. Verani M, Guidry G, Mahmarian J, Shigeyuki N, Theodoros A, Roberts R, et al. Effects of acute, transient coronary occlusion on global and regional right ventricular function in humans. J Am Coll Cardiol 1992;20:1490-7.
49. Gioia G, Lin B, Katz R, Dimarino AJ, Ogilby JD, Cassel D, et al. Use of tantalum-178 generator and a multiwire gamma camera to study the effect of the Mueller maneuver on left ventricular performance: comparison to hemodynamics and single photon emission computed tomography perfusion patterns. Am Heart J 1995;130:1062-7.
50. Ott RJ, Flower MA, Babich JW, Marsden PK. The physics of radioisotope imaging. In: Webb S, editor. The physics of medical imaging. London: Institute of Physics Publishing; 1988. p. 171-5.
51. Iskandrian AS, Verani MS. First-pass radionuclide angiography with a multiwire gamma camera. In: Iskandrian AS, Verani MS, editors. New developments in cardiac nuclear imaging. Armonk (NY): Futura Publishing; 1998. p. 79-93.
52. Iskandrian AS, Verani MS. Nuclear cardiac imaging: principles and applications. Philadelphia: FA Davis; 1996.
53. Hartley CJ, Lacy JL, Dai D, Nayak N, Taffet GE, Entman ML, et al. Functional cardiac imaging in mice using Ta-178. Nature Med 1999;5:237-8.
54. Lacy J, Ball ME, Verani M, Wiles HB, Babich JW, LeBlanc AD, et al. An improved tungsten-178/tantalum-178 generator system for high volume clinical application. J Nucl Med 1988;29:1526-38.
55. Lacy JL, Layne WW, Guidry G, Verani M, Roberts R. Development and clinical performance of automated, portable tungsten-178/tantalum-178 generator. J Nucl Med 1991;32:2158-61.
56. Verani MS, Lacy J, Guidry GW, Nishimura S, Mahmarian JJ, Athanasoulis T, et al. Quantification of left ventricular performance during transient coronary occlusion at various anatomic sites in humans: a study using tantalum-178 and a multiwire gamma camera. J Am Coll Cardiol 1992;19:297-306.
57. National Institutes of Health Office of Science and Health Reports. DHHS Publication No. 85-23. Guide for the care and use of laboratory animals. Washington DC: National Academy Press; 1985.
58. Michael LH, Ballantyne CM, Zachariah JP, Gould KE, Pocius JS, Taffet GE, et al. Myocardial infarction and remodeling in mice: effect of reperfusion. Am J Physiol 1999;277:H660-8.
59. Michael LH, Entman ML, Hartley CJ, Youker KA, Zhu J, Hall SR, et al. Myocardial ischemia and reperfusion: a murine model. Am J Physiol 1995;269:H2147-54.
60. Hartley CJ, Michael LH, Entman ML. Noninvasive measurement of ascending aortic blood velocity in mice. Am J Physiol 1999;268(1 Pt 2):H499-505.
61. Scherrer-Crosbie M, Steudel W, Hunziker PR, Liel-Cohen N, Ullrich WM, Picard MH. Three-dimensional echocardiographic assessment of left ventricular wall motion abnormalities in mouse myocardial infarction. J Am Soc Echocardiogr 1999;12:834-40.
62. Ruff J, Wiesmann F, Hiller K, Voll S, Kienlin M, Bauer WR, et al. Magnetic resonance microimaging for noninvasive quantification of myocardial function and mass in the mouse. Magn Reson Med 1998;40:43-8.